Forschungszentrum Karlsruhe

Technik und Umwelt

Wissenschaftliche Berichte

FZKA 6469

On lateral deflection of the SOL plasma in tokamaks during giant ELMs

I.S. Landman*, H. Würz

Institut für Hochleistungsimpuls- und Mikrowellentechnik

Projekt Kernfusion

* permanent address: Troitsk Institute for Innovation and Fusion Research, 142092 Troitsk, Russia

This work was supported in the frame of the Russian German WTZ cooperation agreement RUS-524-96

Forschungszentrum Karlsruhe GmbH, Karlsruhe
2000

Abstract

In recent H-mode experiments at JET with giant ELMs a lateral deflection of hot tokamak plasma leaving the scrape-off layer and striking the divertor plate has been observed. This deflection can effect the divertor erosion caused by the hot plasma irradiation, because of enlarging the irradiated area. A simplified MHD model of the vapor shield plasma and of the hot plasma initially formed at time $t \to -\infty$ is analyzed. At $t = -\infty$ both plasmas are assumed to stay on rest and to be separated by a boundary, which is parallel to the plate surface. The interaction between plasmas is assumed to develop gradually ('adiabatically') as $\exp(t/t_0)$ with $t_0 \sim 10^2$ μs the ELM duration time. Electrical insulation of the core tokamak plasma is assumed everywhere except for the contact with the divertor. Electric currents are flowing only in the toroidal direction. These currents developing in the interaction zone of the hot plasma and the rather cold target plasma are calculated for inclined impact of the magnetized hot plasma. At such conditions the $\mathbf{J}\times\mathbf{B}$ force in the lateral direction accelerates the interacting plasmas. The motion of the cold plasma and the gradual increase of the plasma interaction intensity are shown to be important for the appropriate deflection magnitude. Adiabatically responding against the increase of the interaction intensity the cold plasma motion compensates significantly the currents thus decreasing the deflection compared to motionless approach. The calculated magnitude of the hot plasma deflection is comparable to the observed one. The results of the modeling are discussed in relation to the experiments. It is shown that sudden switching on of the interaction produces Alfven oscillations of large amplitudes causing much larger amplitudes of the magnetic field induced by the currents than in the adiabatic case.

Zur seitlichen Ablenkung des SOL Plasmas in Tokamaks während großer ELMs

Zusammenfassung

In jüngsten JET H-Mode Experimenten mit ELMs wurde eine seitliche Ablenkung des inneren und äußeren Separatrixauftreffpunktes am Divertor beobachtet. Solche Ablenkungen können die Divertorerosion wegen der Vergrößerung der belasteten Fläche beeinflussen. Es wurde ein analytisches MHD Modell von Dampfschicht und SOL Plasma zur Beschreibung der Plasmaablenkung entwickelt. Dabei wird angenommen, dass beide Plasmen anfangs in Ruhe sind und durch eine ebene Grenzfläche parallel zur Targetoberfläche getrennt sind. Die sich zeitlich entwickelnde Plasmawechselwirkung wird gemaß $\exp(t/t_0)$ mit $t_0 = 100$ µs (Zeitdauer eines ELMs) beschrieben.

Die in der Wechselwirkungszone des heißen einfallenden SOL Plasmas und des kalten Targetplasmas fließenden toroidalen Ströme bewirken zusammen mit dem externen Magnetfeld eine Ablenkung beider Plasmen. Die berechnete Größenordnung der Ablenkung des heißen Plasmas ist in Übereinstimmung mit der gemessenen. Im Gegensatz zum experimentellen Befund geht die berechnete Ablenkung von äußerem und innerem Auftreffpunkt in die gleicher Richtung. Beim plötzlichen Einschalten der Wechselwirkung zwischen den Plasmen treten Alfven Schwingungen großer Amplitude auf. Diese erzeugen Magnetfelder, welche größer sind als im adiabatischen Fall.

CONTENT

1. INTRODUCTION 1

2. EXPERIMENTS ON LATERAL DEFLECTION 2

3. EXISTING DEFLECTION MODELS 3

4. MATHEMATICAL PROBLEM 5

   4.1 Toroidal current 8

   4.2 Propagation of hot electrons in the cold plasma 8

   4.3 Motion of the plasmas 9

   4.4 Currents and electromagnetic field 10

5. ANALYSIS OF THE EQUATIONS 12

   5.1 Solution of the equations 14

   5.2 Sudden start of the plasma interaction 16

   5.3 Adiabatic increase of the interaction intensity 18

6. DISCUSSION 20

7. CONCLUSION 22

8. REFERENCES 23

1. INTRODUCTION

To achieve good plasma confinement the H-mode of operation is used in a tokamak. However in H-mode operation, edge localized modes (ELMs) develop. During one single ELM up to 10% of the thermal energy content of the confined plasma is expelled from the central region inside the separatrix [1]. After crossing the separatrix the expelled hot plasma is lost to the scrape-off layer (SOL) enveloping the confining volume. In the SOL the hot plasma following the inclined magnetic field lines is guided to the divertor. The tokamak geometry including the divertor and the SOL plasma is shown schematically in Fig. 1. The rather high thermal loading of the divertor during the ELMs can result in rather serious divertor damage and in production of considerable amounts of impurities.

A comprehensive numerical simulation of the plasma-wall interaction is done for evaluation of different damages caused by intense pulsed heat loads. Up to now no suggestion has been announced how to absorb the large power density without significant heating of the solid surface, which results in erosion. Thus the goal of the modeling is minimization of erosion. For the ELM of duration of 10^2 μs the eroded material (usually carbon or beryllium) forms a vapor layer in front of the divertor plate. For power densities in the range of MW/cm^2 characterizing large ELMs a 2D code was developed which allows to investigate the hot plasma target interaction [2].

The modeling shows that the interaction of the hot plasma with the vapor decreases the heat load at the wall surface because the hot plasma deposits its power in the vapor and thus increases the vapor temperature till production of multiply ionized ions. Stopping of the hot electrons and the deuteron or triton ions in the vapor plasma significantly decreases the direct irradiation of the wall. Then electron heat conduction and radiation transport in the vapor plasma is the target heat load, which continue to produce erosion. The temperature of the vapor plasma always remains much less than the hot plasma temperature.

In experiments at tokamaks it was observed [3] that during an ELM the position of the confined plasma moves only 1 to 2 cm. But during the initial stage of an ELM the separation of the strike points (see Fig. 1) increases between 20 to 36 cm. More details on the available experimental results on the lateral deflection are given in chapter 2. The observed significant shift of the strike points is important for the investigations of divertor erosion. The heat load area at the divertor plates becomes larger. This favorably reduces the average power density but the accompanying deflection of the cold plasma may reduce the effectiveness of the vapor shield and thus could cause enhanced erosion. According to the modeling results, the plasma-wall interaction is a complicated process showing a non-monotonic dependence of erosion mass from the power density. Moreover, if the deflection of the SOL plasma exceeds the size of the divertor plate then the structure can be overloaded.

Hence the numerical modeling of the plasma-wall interaction has to include the physical phenomenon of the lateral deflection. From the experiments and their interpretation it is unclear which physical mechanism produces the lateral deflection. Nevertheless available theoretical hypotheses should be utilized in order to extract finally an appropriate theory, despite the fact that initially the modeling may be rather speculative.

Up to now two models handling the deflection mechanisms are available [4,5,6]. Both models include the vapor shield and are based on the thermoelectric effect. Despite the vapor shield may not be important for explanation of the lateral deflection, these models are useful in order to estimate the role of shielding in the tokamak reactors and investigate the case of modest shielding. The thermoelectric effect is known as an effect of electric field generated at the boundary of two conductors with different temperatures. In case of a closed electric circuit an electric current develops. The thermoelectric effect depends on the physical nature of the conductors and on the external conditions (e.g. presence of magnetic field **B**). A critical analysis of the theoretical models is given in chapter 3.

In order to elaborate the model described in [5,6] a new and consistent non-stationary model for the lateral deflection is analyzed. Nevertheless the presented approach remains still rather artificial aiming only for a principal explanation. Actually the hot plasma initially heats the unshielded wall. After some time vaporization starts and the vapor layer develops transforming gradually into the cold plasma shield. The thermoelectric effect and thus the lateral deflection accompany this process from the beginning of the vaporization or may be even earlier if to account for the previous sputtering erosion. Such analysis is not the matter of this work being the subject of future numerical simulations. For the sake of simplicity the physical mechanism of the lateral effect is explained starting from an intermediate state with already given plasmas.

In chapter 4 a detailed explanation and a mathematical formulation of the problem are given. In chapter 5 the analysis and the solving of the model equations are completed. In chapter 6 the obtained results and the practical relevance of the model are discussed.

2. EXPERIMENTS ON LATERAL DEFLECTION

According to [1], during giant ELMs the measured impurity radiation flux is too large to prescribe the influx of impurities due to sputtering only thus evaporation has to be accounted for. The toroidal symmetry during ELMs usually is not destroyed [7]. Up to now the SOL plasma temperature T_h and the density n_h have not been measured in ELMs. It is assumed that n_h is of the order of 10^{14} cm^{-3}, the electron temperature T_{he} of several hundreds electronvolts and the ion temperature T_{hi} of several keV. Perhaps at the initial phase of an ELM the electron temperature is of the order of T_{hi}.

Information on properties of the vapor is obtained only from calculation. The code of Ref. 2 recently was used for modeling of the graphite erosion caused by ELMs developing with lower power densities in the existing tokamak installations [8]. A cold plasma temperature of T_c below 10 eV and an electron density of $n_{ce} \approx 10^{15}$ cm^{-3} was obtained in the calculations with a power density of 1 MW/cm^2 at the distance of 10 cm from the plate after 100 μs from the beginning of the ELM.

In one of the giant ELMs of Ref. 3 with target heat loads between 0.1 and 0.3 MW/cm^2 the inner strike point moved inwards for 18 cm and the outer strike point outwards for 2 cm. It was speculated that such a lateral movement occurs due to changes in the magnetic field topology (movement of the separatrix) caused by currents flowing from the SOL plasma onto the plates. However in this case because of the same direction of both currents both strike points should move inwards.

Lateral deflections at much larger target heat loads of 20 MW/cm^2 were measured in another experiment [9] aiming to demonstrate the deflection effect and investigating it in more detail. The aim of this investigation was to check the theoretical prediction of Ref. 5 for the hot plasma deflection at inclined impact onto the vapor shield. In Ref. 9 a cylindrical beam of hot magnetized hydrogen plasma of radius 6 cm with n_h of $3{\cdot}10^{15}$ cm^{-3}, T_{he} of 100 – 200 eV and T_{hi} of 1 keV impacted on an inclined graphite plate installed in the magnetic field of $B \approx 2$ T. During the irradiation time of 40 μs a vapor shield of carbon plasma with temperatures up to 50 eV and electron densities up to $5{\cdot}10^{17}$ cm^{-3} is produced. The influence of the magnetic field inclination angle to the plate surface was checked. At perpendicular impact no lateral deflection was observed. At an inclination angle of 20° deflection of the hot plasma beam of 1 to 2 cm was measured. It was assumed that the deflection occurs mainly at an initial stage of the pulse due to the influence of currents crossing the plate surface.

The mentioned experimental facts can be summarized as follows:

1. The deflection occurs only due to the inclination of **B** (Ref. 9).
2. The strike points move mainly before the power flux pulse arrived (Ref. 3). In Ref. 9 a similar guess was mentioned. This finding supports the assumption for a deflection of the hot plasma even without vapor shield. Because the initial stage is most important, models with common T_h for the SOL plasma particles seem reasonable for first steps of the modeling. Then dynamics of T_{he} has to be taken into account at the next steps as it is the most critical parameter of the hot plasma.
3. It seems that the deflection increases with increasing power density because of larger deflection at the inner strike point (Ref. 3). Clearly, the case of Ref. 9 where despite larger target power density of the plasma beam a lower deflection was obtained compared to the tokamak experiment is in collision with this assumption. But these cases may not be comparable quantitatively because of very different geometry and the hot plasma parameters.
4. The strike points move in the opposite directions buzzing off each other (Ref. 3).
5. During ELMs the toroidal symmetry is valid (Ref. 7). Note that in Ref. 1 the asymmetry was also mentioned concerning the interaction with the structure. It seems that in modeling the symmetry assumption is reasonable.
6. The confined tokamak plasma itself doesn't influence the lateral deflection because its position changes negligibly (Ref. 3).
7. The currents of 0.1 kA/cm^2 through the divertor plate surface measured in Ref. 3 are not principally important for the lateral effect.

3. EXISTING DEFLECTION MODELS

For the hot plasma and the cold plasma conductors initially the perpendicular impact of the hot plasma onto the cold plasma was considered [10], aiming for elaboration of electrostatic stopping for the hot electrons. The impacting hot plasma ions have a rather short range in the cold plasma. The hot electrons propagate much deeper into the cold plasma region undergoing weak collisions on their stopping length λ_e. Electric currents in the plasma are assumed to be absent. Thus in the cold plasma an

electron flux appears compensating the flux of the hot electrons. As a consequence an electric field **E** develops in the cold plasma because in accordance with Ohms law the cold electron flux is possible only due to an electric field **E**. The potential barrier of **E** effectively slows down the hot electrons but their penetration distance remains larger than that of the ions.

In Refs. 4, 5 and 6 the idea is exploited that in case of the inclined **B** the field **E** becomes non-parallel to **B** resulting in the lateral motion due to the **E**×**B** drift. In Ref. 4 only the drift deflection of the cold plasma was analyzed and in Refs. 5 and 6 only the drift deflection of the hot plasma.

Before start of an ELM the SOL volume up to the plate surface is assumed to be empty, filled with a homogeneous, stationary inclined magnetic field $\mathbf{B}_0$ without electric field. Generally electric currents of current densities **J** flowing in the plasma produce an electric field **E** and perturbations $\delta\mathbf{B}$ of the magnetic field given via the whole field **B** as $\mathbf{B} = \mathbf{B}_0 + \delta\mathbf{B}$. The induced fields **E** and $\delta\mathbf{B}$ obey the Maxwell equations as

$$\mathrm{rot}\mathbf{E} = -\frac{1}{c}\frac{\partial\delta\mathbf{B}}{\partial t} \tag{1}$$

$$\mathrm{rot}\delta\mathbf{B} = \frac{4\pi}{c}\mathbf{J} \tag{2}$$

with c the speed of light in vacuum. In Eqs. (1) and (2) the current density is seen as the source for the field production. The electric field is split into the potential field $\mathbf{E}_\phi$ and the vortex field $\mathbf{E}_\upsilon$ as $\mathbf{E} = \mathbf{E}_\upsilon + \mathbf{E}_\phi$. The vortex field is obtained from Eq. (1) with the time derivative of $\delta\mathbf{B}$ being the source for $\mathbf{E}_\upsilon$. The potential field is given as $\mathbf{E}_\phi = -\mathrm{grad}\phi$ with ϕ the electric potential. In the thin boundary sheath the potential is obtained from the Poisson equation $\Delta\phi = 4\pi e(n_e - Zn_i)$ with e the elementary charge and Z the mean charge state. In the main plasma volume the quasineutrality equation is valid as $n_e = n_i = n_h$ for the hot plasma and $n_e \equiv n_{ce} = Zn_{ci} \equiv Zn_i$ for the cold plasma. The quasineutrality equation is used to obtain ϕ in the main volume.

In Ref. 4 the electric field is assumed to be given as $\mathbf{E} = \mathbf{E}_\phi = -\nabla\phi$ thus $\mathbf{E}_\upsilon \equiv 0$. It is valid $\mathrm{rot}\mathbf{E}_\phi \equiv 0$ resulting in $\delta\mathbf{B} = 0$ according to Eq. (1). Because **J** obeys Eq. (2), the current **J** is zero. Thus currents flowing in the cold plasma are neglected and any influence of them on the behavior of the hot plasma is not considered.

In Refs. 5 and 6 an attempt is made to explain the motion of the hot plasma for the first time considering the plasma interaction as a non-stationary process with $\partial\delta\mathbf{B}/\partial t \neq 0$. This model, based on a kinetic description of the hot plasma, includes the electrostatic sheath and the magnetic pre-sheath at the boundary of the plasmas. The sheath problem is separated from the problem of the lateral motion. In order to simplify the analysis the density of the cold plasma ρ_c is assumed to be much larger than the density of the hot plasma ρ_h as $\rho_c/\rho_h \to \infty$. Thus the motion of the cold plasma is prohibited because of its infinite inertia. By this way the reason for the lateral motion of the hot plasma has been discovered. It is the penetration of the electromagnetic field through the boundary between the plasmas.

As is shown in Ref. 5, a toroidal current of the density $\mathbf{J} \neq 0$ flowing in the cold plasma accompanies the thermoelectric effect at the inclined plasma interaction. In accordance with Eq. (2) the perturbation $\delta\mathbf{B}$ develops during the interaction of the plasmas. Assuming the penetration of $\delta\mathbf{B}$ through the boundary a vortex contribution $\mathbf{E}_\upsilon$ to $\mathbf{E}$ with a non-zero projection onto $\mathbf{B}$ is obtained from Eq. (1) in the hot plasma. It is assumed $T_h >> T_c$. Electric conductivity of the hot plasma is much larger than that of the cold plasma. For this reason the hot plasma conductivity is assumed to be infinitely large. As it is known, the projection of $\mathbf{E}$ onto $\mathbf{B}$ is equal to zero in the conductors of infinite conductivity being on rest. In such conductors $\mathbf{E}$ is perpendicular to $\mathbf{B}$ thus it is valid $\mathbf{EB} = 0$. Because it is valid $\mathbf{E} = \mathbf{E}_\upsilon + \mathbf{E}_\phi$ with $\mathbf{E}_\upsilon\mathbf{B} \neq 0$, for the hot plasma on rest it follows $\mathbf{E}_\phi\mathbf{B} \neq 0$. Thus due to the primordial toroidal current in the cold plasma a vortex and a potential field develops in the hot plasma. At small inclination angle α given as $\alpha << 1$ it was obtained that $\mathbf{E}_\phi$ becomes much larger than $\mathbf{E}_\upsilon$ and is directed almost perpendicularly to $\mathbf{B}_0$. It is concluded that a lateral motion of the hot plasma occurs due to an $\mathbf{E}\times\mathbf{B}$ drift with the lateral velocity given as $\mathbf{V} \approx c\mathbf{E}_\phi\times\mathbf{B}_0/B^2$. Hence despite the mentioned precondition for the hot plasma to be on rest it was obtained afterwards that the hot plasma moves. In this aspect the model of Ref. 5 is not consistent.

In the model of Ref. 4 according to Fig. 1 the potential electric field behaves similarly near both strike points. Because it slows down the hot electrons coming to the divertor plate, in Fig. 1 the vectors of $\mathbf{E}_\phi$ would be directed down (not shown). The toroidal component $\mathbf{B}_z$ of the magnetic field dominates thus the drift velocity is given approximately as $\mathbf{V}_d \approx c\mathbf{E}_\phi\times\mathbf{e}_z/B$ with $\mathbf{e}_z$ the constant unit vector towards $\mathbf{B}_z$. Due to the same direction of $\mathbf{E}_\phi$ for both strike points this expression gives the same direction for the lateral velocity, which results in shifts of the same direction for both strike points.

In the model of Ref. 5 the direction of the toroidal current in the cold plasma depends on the direction of the poloidal component of $\mathbf{B}$. The poloidal field direction is shown in Fig. 1 as the direction of x-axis being reverse for the inner and outer strike points. Thus the vectors $\mathbf{J}$ near the different strike points are of opposite signs. If changing the sign of $\mathbf{J}$ in Eqs. (1) and (2), the sign of $\delta\mathbf{B}$ and $\mathbf{E}_\upsilon$ also changes. Because in the hot plasma from the above mentioned equality $\mathbf{EB} = 0$ with $\mathbf{E} = \mathbf{E}_\upsilon + \mathbf{E}_\phi$ follows the equality $\mathbf{E}_\phi\mathbf{B}_0 \approx -\mathbf{E}_\upsilon\mathbf{B}_0$, the sign of $\mathbf{E}_\phi$ changes, too. Thus $\mathbf{V}_d$ there has opposite signs near the different strike points resulting in reversed shifts of the strike points as it is in the experiment. This favorable feature of the model triggered further investigations of the deflection effect being described below.

4. MATHEMATICAL PROBLEM

In the presented analysis the motion of both plasmas is taken into account. The condition that the hot plasma is at rest, which was mentioned in chapter 3, is used only as the initial condition for solving the differential equations but not more as the pre-assumption for the permanent state of the plasmas. The previously obtained results for the sheaths are used. Due to this the kinetic description is not necessary. The lateral effect is analyzed with the MHD approach for both plasmas. The drift approach becomes not necessary because the lateral velocity is one of the variables in the MHD equations.

The model considers interaction of two toroidal plasmas initially being on rest and immersed into a magnetic field inclined to the boundary between the plasmas. At the boundary an electromagnetic layer of increasing thickness forms in order to prevent free mutual penetration of the plasmas. The plasmas are assumed to be limited in all directions and thus to have the sizes a_x, a_y and a_z with different a_x for the hot and the cold plasmas. The initial positions of the plasmas are shown schematically in Fig. 2. The initial separating boundary is given as a surface at $x = 0$ with x the coordinate of variation of plasma parameters. At $x < 0$ the cold plasma of the temperature T_c and the ion density n_c and at $x > 0$ the hot plasma of T_h and n_h are given. For other two coordinates (y and z) the translation symmetry in y-direction and the toroidal symmetry in z-direction is assumed ($\partial/\partial y = 0$, $\partial/\partial z = 0$). Due to the lateral motion the plasma edge in y-direction shifts thus a_y gets to be a function of x. The initial magnetic field is given as $\mathbf{B}_0 = (B_x,0,B_z)$ with $B_x = B_0\sin\alpha$, $B_z = B_0\cos\alpha$ and α the inclination angle.

For practical estimations a deuterium hot plasma and a graphite plate in the inclined magnetic field of $B_0 = 5$ T and $\alpha = 0.1$ rad are used. Thus the magnetic field is rather parallel to the z-direction. The cold plasma is the ionized vapor layer of the wall material adjacent to the wall surface. Typical values of T_c, T_h and n_h are chosen as $T_c = 30$ eV, $T_h = 3$ keV and $n_h = 3\cdot10^{13}$ cm^{-3}.

After exclusion of the electrostatic sheath from the analysis the plasmas get quasineutral thus the electric charge of the plasmas is negligibly small. Assuming that the hot plasma is insulated at $x = a_x$ e.g. by vacuum or due to additional symmetry requirements it is concluded that the current cannot penetrate in the x-direction. Therefore for the current density $\mathbf{J} = (J_x,J_y,J_z)$ it is valid $J_x = 0$. With the vacuum edge in y-direction the y-component J_y is also forbidden. According to Fig. 1 this condition seems quite natural for the regions located under the X-point. Above the X-point the vacuum is assumed only for the outer shell of SOL, which remains to be sufficient for the condition of $J_y = 0$.

In the toroidal geometry the current still has the possibility to flow thus J_z will be not equal to zero if there is a generator of the toroidal current in the plasmas. The thermoelectric current generation results from the interaction of the toroidal plasmas in the inclined magnetic field. The electrons of the hot plasma before stopping in the cold plasma penetrate rather deeply into it along the magnetic field lines. In the inclined magnetic field the compensation of x-component of the hot electron current by the reversed current of the cold plasma electrons, which obey the Ohms law, results in an electric field with a non-zero z-component. In the toroidal geometry the z-component of the electric field forms a vortex field E_z with closed field lines. Hence according to Eq. (1) for producing of E_z the additional y-directed magnetic field B_y and the toroidal current of the density J_z are required. As a result $\delta\mathbf{B}$ and $\mathbf{J}$ are represented as $\delta\mathbf{B} = (0,B_y,0)$ and $\mathbf{J} = (0,0,J_z)$. The radiuses of the current loops are assumed to be large enough for neglecting complications caused by the toroidal metric. Thus the analysis is completed in the Cartesian geometry with the homogeneous and stationary $\mathbf{B}_0$.

Because the process is principally non-stationary, the final magnitude of the deflection depends significantly on the kind of development of the plasma interaction. The magnitude J_{he} of the hot electron current in the cold plasma characterizes the intensity of the interaction. Two different ways of changing J_{he} in time are considered and

compared. Those are an immediate plasma contact after initial time moment of $t = 0$ and a gradual ('adiabatic') contact beginning at infinitely early moment of $t = -\infty$.

The start of the interaction at time $t = 0$ with J_{he} suddenly changing from zero up to its maximum value allows to consider unlimited in the x-direction plasmas for a short interaction time at which the thickness of plasma interface remains much smaller than a_x. In order to avoid non-principal complexity only the solution at rather small distances from the boundary $|x| << \lambda_e \sin|\alpha|$ is analyzed. The analysis of the sudden switching on case is used for physical interpretation of the deflection effect.

Adiabatic switching on an exponential factor $\exp(t/t_0)$ is used in J_{he} with t_0 the characteristic interaction time and final moment of the interaction assumed at $t = 0$. In the estimations the value of $t_0 = 100$ μs is applied. This case presents the solution adequately fitting to the experimental conditions in the frame of the assumptions of the analyzed model.

In the one-dimensional problem with the adiabatic increase of J_{he} the plasma edge in x-direction is important. The edge is modeled by the planes of $x = -L_c$ and $x = L_h$ i.e. with $a_x = L_c$ for the cold plasma and $a_x = L_h$ for the hot plasma. The hot electrons are allowed to penetrate into the plane at $x = -L_c$ because it is assumed that afterwards they get absorbed by the wall. In order to simulate the plasma interaction with the edge, the boundary conditions are defined as follows: because at $x = -L_c$ the wall stops the plasma motion, the lateral velocity V_y is assumed to vanish there. The plane of $x = L_h$ is assumed to simulate the middle plane of SOL in relation to which the lateral deflection is symmetrical. Thus V_y is assumed to be symmetrical. This requirement results in the zero condition for the spatial derivative $\partial V_y/\partial x$. Hence the boundary conditions for the plasmas are given as

$$V_y\Big|_{x=-L_c} = 0, \qquad \frac{\partial V_y}{\partial x}\Big|_{x=L_h} = 0 \tag{3}$$

Note that the choice of the boundary conditions of Eq. (3) at $x = L_h$ depends on the analysis of a more general problem including two strike points. If implying to apply the considered one-dimensional model for interpretation of the experimentally obtained results, the alternative choice may be with $V_y|_{x=Lh} = 0$. The influence of such change of the boundary condition is discussed in chapter 6.

All other main assumptions, which were mentioned in Ref. 5, are assumed to be valid. They are a large difference of the hot and cold plasma temperatures ($T_h >> T_c$), infinite electric conductivity of the hot plasma and isotropy approximation for the cold plasma conductivity. At $T_h >> T_c$ the following consequences are valid. Stopping length λ_e of the hot electrons in the cold plasma is much larger compared to that of the hot ions. Potential drop ϕ_0 over the sheath located at the boundary is estimated as $\phi_0 = T_h/e$. n_h is small compared to n_c and the cold plasma electron density n_{ce} as $n_h << n_c, n_{ce}$. Thus the pressure balance condition after neglecting a small contribution of the hot electrons in the cold plasma is given as $(n_c + n_{ce})T_c \approx 2n_hT_h$. Due to the plasma quasineutrality it is valid $n_{ce} \approx Zn_c$. The estimation $Z = 5$ for the charge state is applied, which is typical in case of graphite target.

4.1 Toroidal current

The hot particles propagate towards the plasma boundary until crossing the sheath at $x = 0$. Then the hot ions are stopped near the boundary. Their accumulation is compensated by diffusion back to the hot plasma. But the hot electrons penetrate into the cold plasma along the magnetic field lines rather deeply. Finally the hot electrons also loss their energy and join the cold electrons. In order to avoid accumulation of positive electric charges in the hot plasma an electric field develops in the cold plasma slowing down the hot electrons there and forcing the cold electrons to compensate the positive charge. Together with the sheath potential drop this constitutes the mechanism of the thermoelectric effect for the considered two plasmas.

The current densities of the hot and cold electrons are related with the ion fluid velocity $\mathbf{V}$ as $\mathbf{J}_{he} = en_{he}(\mathbf{V} - \mathbf{V}_{he})$ and $\mathbf{J}_{ce} = en_{ce}(\mathbf{V} - \mathbf{V}_{ce})$ where $\mathbf{V}_{he}$ and $\mathbf{V}_{ce}$ are the electron fluids velocities. The vector $\mathbf{V}_{he}$ is represented as $\mathbf{V}_{he} = \mathbf{V}_{he\|} + \mathbf{V}_{he\perp}$ by its parallel and perpendicular projections onto $\mathbf{B}$. It is assumed that $V_{he\|}$ is given as J_{he}/en_{he}. The $\mathbf{E}\times\mathbf{B}$ drift determines $\mathbf{V}_{he\perp}$ as $\mathbf{V}_{he\perp} = c(\mathbf{E}\times\mathbf{B})/B^2$.

Initially $\mathbf{V}$ is equal to zero. If neglecting $\mathbf{V}_{he\perp}$, the hot electron current directs along $\mathbf{B}$. At the inclination angle $\alpha \neq \pi/2$ the compensating current of the collisional cold electrons may cross the magnetic field lines significantly. E.g. in case of very fast collisions the cold electrons would be not magnetized. The non-magnetized cold electrons compensate the charge of the stopped ions moving rather perpendicularly to the plasma boundary but not along $\mathbf{B}$. An intermediate case is shown in Fig. 3 demonstrating that the current density $\mathbf{J}_{ce}$ of the cold electrons is always less inclined to the boundary than $\mathbf{J}_{he}$. Rigorous analysis including $\mathbf{V} \neq 0$ and $\mathbf{V}_{he\perp} \neq 0$ is carried out in chapter 5. The x-and y-components of $\mathbf{J}_{ce}$ compensate those of $\mathbf{J}_{he}$ as

$$J_{hex} + J_{cex} = 0, \qquad J_{hey} + J_{cey} = 0 \tag{4}$$

Hence only a toroidal current with current density $J_z = J_{hez} + J_{cez}$ develops at $x < 0$.

The sign of J_z depends on the sign of B_x. According to Figs. 3a and 3b if changing the sign of B_x the direction of propagation of the hot electrons along $\mathbf{B}$ and thus that of $\mathbf{J}_{he}$ also changes resulting in the change of the sign of J_z, which was already mentioned explaining the model of Ref. 5.

4.2 Propagation of hot electrons in the cold plasma

A beam penetrating into the cold plasma after crossing the boundary sheath models the impinging hot electrons at $x < 0$. Inside the cold plasma the hot electron beam gradually gets to stop. The density n_{he} and the current magnitude J_{he} at $x < 0$ are modeled using the Boltzmann distribution for the hot electrons as

$$n_{he} = \frac{n_h}{2}\exp\left(-\frac{l}{\lambda_e} - \frac{U(x)}{T_h}\right), \qquad J_{he} = \frac{e\upsilon_{The}n_{he}}{\sqrt{\pi}} \tag{5}$$

with $l > 0$ the distance along a magnetic field line in the cold plasma from the boundary, $\upsilon_{The} = (2T_h/m_e)^{1/2}$ the thermal velocity of the hot electrons and m_e the electron mass. The switching on factor is omitted in Eq. (5). The stopping effect is modeled by the exponential factor $\exp(-l/\lambda_e)$. The electron potential energy $U(x)$ consists of the sheath potential barrier ϕ_0 and the slowing down 'effective potential' φ as

$$U(x) = e\phi_0 - e\varphi(x) \quad \text{with } \varphi(x) = \int_0^{l(x)} E_{\|}(l')dl' \tag{6}$$

where $E_{\|}$ is the projection of the electric field strength **E** onto **B**. The effective potential includes contributions of both vortex and potential electric fields $\mathbf{E}_\upsilon$ and $\mathbf{E}_\phi$.

The coordinate l is conveniently expressed as a function of x via α and the angle γ between the vectors **B** and $\mathbf{B}_0$ given as $\gamma = \arctan(B_y/B_0)$. The value of B is expressed as $B = B_0/\cos\gamma$. Always it is assumed that $B_z > 0$. If it is valid $B_x > 0$ and thus $\alpha > 0$, l–axis is directed reversely to **B**. Otherwise the l–axis is directed as **B** (see Fig. 3). Therefore for differentials of the variables $\mathbf{r} = (x,y,z)$ and l along the l–axis it is valid $d\mathbf{r} = -s_\alpha(\mathbf{B}/B)dl$ with $s_\alpha = 1$ at $\alpha > 0$ and $s_\alpha = -1$ at $\alpha < 0$. In terms of dl and $d\mathbf{r}$ the differential of the effective potential is given as $d\varphi = E_{\|}(l)dl = -\mathbf{E}d\mathbf{r}$ with $\mathbf{E} = (E_x,E_y,E_z)$ a vector-function of x. Thus it is valid $d\varphi = s_\alpha(\mathbf{EB}/B)dl$. Final expressions for dl and φ are obtained as

$$dl = -\frac{dx}{\cos\gamma\sin|\alpha|}, \qquad \varphi(x) = \int_x^{x_b} \frac{\mathbf{EB}}{B_0}\frac{dx}{\sin\alpha} \tag{7}$$

The function $x_b(t)$ is the x-coordinate of the boundary.

Below it is shown that B_y is small compared to B_0. From this follows that γ is also small and the plasma density keeps constant resulting in plasma immobility in x-direction. Therefore the simplifications $x_b = 0$, $\cos\gamma = 1$ and $\sin^2\gamma = 0$ are used but the small terms with $\sin\gamma$ are not neglected. Due to this it is obtained the relation between the coordinates l and x as $l = -x/\sin|\alpha|$.

4.3 Motion of the plasmas

The lateral plasma motion is described by the Euler equation as

$$\rho\frac{\partial V_y}{\partial t} = \frac{B_x J_z}{c}, \qquad V_y\big|_{\text{init}} = 0 \tag{8}$$

with V_y the ion lateral velocity and index 'init' denoting initial values. Below for the different plasmas the designations are supplied by additional indexes as $\rho = \rho_c$ or $\rho = \rho_h$. For each plasma the initial density is assumed to be homogeneus. Because practically only the lateral motion occurs, from the continuity equation $\partial\rho/\partial t + \nabla\rho\mathbf{V} = 0$ with

$\mathbf{V} = (0,V_y,0)$ the plasma velocity vector, and from the assumption $\partial/\partial y = 0$ for the lateral direction follows that the plasma density doesn't change during the process thus remaining homogeneous. The magnitude of the lateral deflection Δ_y is given by the time integration of V_y as

$$\Delta_y(t,x) = \int_{t_{\text{init}}}^{t} V_y(t',x)dt' \tag{9}$$

From Eq. (8) follows that the direction of the deflection of the cold plasma remains the same independently on the sign of B_x. Because in accordance with Fig. 3 the current in the cold plasma changes its sign simultaneously with that of B_x. Hence near both the strike points of Fig. 1 the cold plasma deflects in the same direction along the divertor plate.

4.4 Currents and electromagnetic field

According to Eq. (2) the induced magnetic field B_y is related with the current density J_z as

$$\frac{\partial B_y}{\partial x} = \frac{4\pi}{c} J_z \tag{10}$$

From Eq. (1) follows that the evolution of B_y is determined by the vortex electric field E_z as

$$\frac{\partial B_y}{\partial t} = c\frac{\partial E_z}{\partial x}, \qquad B_y\Big|_{\text{init}} = 0 \tag{11}$$

In order to fit the fields at the boundary between the hot and cold plasmas the continuity of B_y and E_z across the boundary is required. The solution of Eqs. (10) and (11) is determined by the boundary conditions at the plasma edge at $x = -L_c$ and $x = L_h$. At $x = -L_c$ the boundary condition for B_y follows from Eqs. (3) and (8) with non-zero B_x. It is obtained $\partial B_y/\partial x|_{x=-Lc} = 0$. The expression for the boundary condition at $x = L_h$ in terms of the magnetic field is derived below.

The relation between the current density $\mathbf{J}$ and the fields $\mathbf{E}$ and $\mathbf{B}$ is described by Ohm's law as

$$\mathbf{J} = \sigma\left(\mathbf{E} + \frac{1}{c}\mathbf{V}_e \times \mathbf{B}\right) \tag{12}$$

with σ the electric conductivity and $\mathbf{V}_e$ the electron fluid velocity. For the hot and cold plasmas Ohm's law gets different forms. In the collisionless hot plasma region ($\sigma = \infty$) it

follows from Eq. (12): $\mathbf{E} + \mathbf{V}_{he} \times \mathbf{B}/c = 0$ with $\mathbf{V}_{he} = \mathbf{V} - \mathbf{J}/en_h$ the fluid velocity of the hot electrons. Excluding $\mathbf{V}_{he}$ the components of $\mathbf{E}$ for the region of $x > 0$ are obtained as

$$E_x = -\frac{V_y B_z}{c} - \frac{J_z B_y}{cen_h}, \qquad E_y = \frac{J_z B_x}{cen_h}, \qquad E_z = \frac{V_y B_x}{c} \tag{13}$$

From Eq. (13) follows $E_{\|} = 0$. From Eq. (6) applied there with $l(x) < 0$ follows $\varphi = 0$ in the hot plasma.

In the cold plasma the current density consists of contributions of the hot and cold electrons as $\mathbf{J} = \mathbf{J}_{he} + \mathbf{J}_{ce}$ (see Fig. 3). The hot electron current is given as $\mathbf{J}_{he} = s_\alpha J_{he}\mathbf{B}/B - en_{he}c(\mathbf{E}\times\mathbf{B})/B^2$. The cold electron current is given by Eq. (12) as $\mathbf{J}_{ce} = \sigma_c(\mathbf{E} + \mathbf{V}_{ce}\times\mathbf{B}/c)$ with $\mathbf{V}_{ce} = \mathbf{V} - \mathbf{J}_{ce}/en_{ce}$ the fluid velocity of the cold electrons and σ_c the cold plasma conductivity. Multiplying the expression for $\mathbf{J}_{ce}$ by $\mathbf{B}$ and then excluding $\mathbf{J}_{ce}$, as it is equal to $\mathbf{J} - \mathbf{J}_{he}$, the scalar product $\mathbf{EB}$ is obtained as

$$\mathbf{EB} = \frac{\mathbf{BJ}}{\sigma_c} - \frac{s_\alpha J_{he}}{\sigma_c} B \quad (x < 0) \tag{14}$$

Substituting $\mathbf{EB}$ of Eq. (14) into Eq. (8) and using Eq. (10) the effective potential is obtained as

$$\varphi = \Phi + \frac{c\cot\alpha}{4\pi\sigma_c}\left(B_y\big|_{x=x_b} - B_y\right) \tag{15}$$

with the function $\Phi(x)$ given as

$$\Phi = \frac{1}{\sigma_c \sin|\alpha|}\int_{x_b}^{x} J_{he}(x')\frac{dx'}{\cos\gamma} \tag{16}$$

The hot electron current is conveniently expressed via Φ as

$$J_{he} = \sigma_c \sin|\alpha|\cos\gamma\frac{\partial\Phi}{\partial x} \tag{17}$$

According to Eq. (14) the electric field is represented as $\mathbf{E} = \mathbf{E}_\perp + \mathbf{E}_{\|}$ with $\mathbf{E}_{\|} = (\mathbf{B}/B)(\mathbf{BJ} - s_\alpha J_{he}B)/(\sigma_c B)$. Excluding consequently $\mathbf{V}_{ce}$, $\mathbf{J}_{ce}$ and $\mathbf{J}_{he}$ from Ohm's law at $x < 0$, the equation for $\mathbf{E}_\perp$ in the cold plasma is obtained as

$$\mathbf{E}_\perp = \mathbf{W}\times\mathbf{B} - \frac{n_{he}}{n_{ce}}\mathbf{E}_\perp + \frac{en_{he}c}{\sigma_c B^2}\mathbf{E}_\perp\times\mathbf{B} \tag{18}$$

with $\mathbf{W} = \mathbf{J}/(cen_{ce}) - \mathbf{V}/c + \mathbf{B}\times\mathbf{J}/(\sigma_c B^2)$. Using the smallness of n_{he} compared to n_{ce}, Eq. (18) is solved approximately by the perturbation method. Replacing $\mathbf{E}_\perp$ in rhs of Eq. (18) by the first term of the rhs, the solution is obtained as

$$\mathbf{E}_\perp \approx \mathbf{W}\times\mathbf{B} + \frac{n_{he}}{n_{ce}}\left(\frac{en_{ce}c}{\sigma_c B^2}\mathbf{W}\times\mathbf{B} - \mathbf{W}\right)\times\mathbf{B} \tag{19}$$

As a result the x-, y- and z-components of $\mathbf{E}$ are obtained as

$$E_x \approx -\frac{V_y B_z}{c} - \frac{s_\alpha J_{he} B_x}{\sigma_c B} - \frac{J_z B_y}{cen_{ce}}, \qquad E_y \approx -\frac{s_\alpha J_{he} B_y}{\sigma_c B} + \frac{J_z B_x}{cen_{ce}} \tag{20}$$

$$E_z = \frac{V_y B_x}{c} - \frac{s_\alpha J_{he} B_z}{\sigma_c B} + \frac{J_z}{\sigma_c} + \Delta E_z \tag{21}$$

$$\Delta E_z = -\frac{n_{he}}{n_{ce}}\left(\frac{en_{ce}c}{\sigma_c B}\frac{B_y}{B}\frac{V_y B_z}{c} + 2\frac{J_z}{\sigma_c}\left(1 - \frac{B_z^2}{B^2}\right) + \frac{B_x V_y}{c}\right) \tag{22}$$

In Eq. (20) bulky terms ΔE_y and ΔE_z, which are proportional to n_{he}, are omitted. In Eq. (21) the small term ΔE_z is kept in order to check its significance for the results. Below it is shown that ΔE_z is negligibly small. Note that the neglecting of $\Delta\mathbf{E}$ is equivalent to the neglecting of the $\mathbf{E}\times\mathbf{B}$ drift term in $\mathbf{J}_{he}$.

5. ANALYSIS OF THE EQUATIONS

Using Eqs. (8) and (10) the current J_z is excluded thus relating B_y and V_y as

$$\rho\frac{\partial V_y}{\partial t} = \frac{B_x}{4\pi}\frac{\partial B_y}{\partial x}, \qquad V_y\big|_{\text{init}} = 0 \tag{23}$$

Using Eq. (17) the function J_{he} is excluded from the system being replaced by Φ. Instead of Φ the dimensionless function $w = e\Phi/T_h$ is conveniently used. Substituting J_{he} of Eq. (5) into Eq. (17) with φ given by Eq. (15) the equation for w in approximation of $x_b = 0$ and $\cos\gamma \approx 1$ is obtained as

$$\frac{\partial w}{\partial x} = \frac{e^2 \upsilon_{The} n_h \exp(-e\phi_0/T_h)}{2\sqrt{\pi}\sigma_c T_h \sin|\alpha|}\exp\left(\frac{x}{\lambda_e \sin|\alpha|} + w + \frac{ec\cot\alpha}{4\pi\sigma_c T_h}\left(B_y\big|_{x=0} - B_y\right)\right) \tag{24}$$

According to Eq. (16) the boundary condition $w|_{x=0} = 0$ is valid. Neglecting the last term in the exponent of Eq. (24), which contains the contribution of B_y, this equation is solved analytically. The solution w is obtained as

$$w(x) = -\ln\left(1 + K\left(1 - \exp\left(sx/L_h\right)\right)\right) \tag{25}$$

The dimensionless constants K and s are given as

$$K = \frac{e^2 \lambda_e \upsilon_{The} n_h \exp\left(-e\phi_0/T_h\right)}{2\sqrt{\pi}\sigma_c T_h}, \qquad s = \frac{L_h}{\lambda_e \sin|\alpha|} \tag{26}$$

Using Eq. (11) with E_z of Eqs. (13) and (21), neglecting ΔE_z, after substituting J_{he} of Eq. (17) and J_z of Eq. (10) with $\cos\gamma \approx 1$, the equation for B_y is obtained as

$$\frac{\partial B_y}{\partial t} - B_x \frac{\partial V_y}{\partial x} = \left[\begin{array}{c} \dfrac{\partial}{\partial x}\left(\dfrac{c^2}{4\pi\sigma_c} \dfrac{\partial B_y}{\partial x} - \dfrac{cT_h}{2e} \sin 2\alpha \dfrac{\partial w}{\partial x} g(t) \right), \; x < 0 \\ 0, \quad x > 0 \end{array} \right] \tag{27}$$

with $B_y|_{\text{init}} = 0$ and the switching on factor g(t) added for the first time. In case of the sudden switching on it is valid $g(t) = \theta(t)$ with the step-function $\theta(t) = 0$ at $t < 0$ and $\theta(t) = 1$ at $t \geq 0$. In the adiabatic case it is valid $g(t) = \exp(t/t_0)$.

As was discussed in chapter 4.4, the boundary condition $\partial B_y/\partial x|_{x=-Lc} = 0$ is valid. As follows from Eqs. (11) and (13), the condition $\partial V_y/\partial x|_{x=Lh} = 0$ of Eq. (3) is equivalent to the equality $\partial B_y/\partial t|_{x=Lh} = 0$ and thus the boundary condition $B_y|_{x=Lh} = 0$ is valid. Eq. (27) requires also the fitting at $x = 0$. Integrating Eqs. (23) and (27) over a small interval across the boundary the fitting conditions are obtained as

$$B_y(-0) = B_y(+0) \tag{28}$$

$$\left(B_x V_y + \frac{c^2}{4\pi\sigma_c} \frac{\partial B_y}{\partial x} - \frac{cT_h}{2e} \sin 2\alpha \frac{\partial w}{\partial x} g \right)\Bigg|_{-0} = B_x V_y \Big|_{+0} \tag{29}$$

Eqs. (28) and (29) express the continuity of B_y and E_z at $x = 0$.

Hence the system of equations to be solved is reduced to Eqs. (23), (24) and (27) for V_y, w and B_y. Assuming a small B_y, Eq. (25) for w is used. In this case the system is linear, and due to this analytical solutions of the problem are obtained.

The functions $B_y(t,x)$ and $V_y(t,x)$ are conveniently replaced by the dimensionless functions $b(\tau,\xi)$ and $\upsilon(\tau,\xi)$ as $B_y = \mu B_0 b$ and $V_y = \mu V_A \upsilon$ with τ and ξ dimensionless time and coordinate, V_A the Alfven velocity of the hot plasma and μ the dimensionless constant given as

$$\tau = \frac{t}{t_0}, \qquad \xi = \frac{x}{L_h}, \qquad \mu = \frac{cT_h t_0 \cot|\alpha|}{eB_0 \lambda_e^2}, \qquad V_A = \frac{B_0}{\sqrt{4\pi\rho_h}} \quad (30)$$

Transforming Eqs. (23), (27), (3), (28) and (29) to the dimensionless variables it is obtained

$$\eta^2 a \frac{\partial \upsilon}{\partial \tau} = s_\alpha \frac{\partial b}{\partial \xi} \ \ (\xi < 0), \qquad a \frac{\partial \upsilon}{\partial \tau} = s_\alpha \frac{\partial b}{\partial \xi} \ \ (\xi > 0), \qquad \upsilon\big|_{\text{init}} = 0 \quad (31)$$

$$\frac{\partial b}{\partial \tau} - \frac{s_\alpha}{a}\frac{\partial \upsilon}{\partial \xi} = \begin{bmatrix} \dfrac{q-1}{a^2\eta^2}\dfrac{\partial^2 b}{\partial \xi^2} - s_\alpha \dfrac{\partial^2 w(L_h\xi)}{s^2 \partial \xi^2} g(t_0\tau), \xi < 0 \\ 0, \quad \xi > 0 \end{bmatrix}, \qquad b\big|_{\text{init}} = 0 \quad (32)$$

$$\upsilon(\tau, -l_c) = 0, \quad \frac{\partial \upsilon}{\partial \xi}(\tau, 1) = 0, \quad b(\tau, -0) = b(\tau, +0) \quad (33)$$

$$\left(\upsilon + s_\alpha \frac{q-1}{a\eta^2}\frac{\partial b}{\partial \xi} - a s^{-2} \frac{\partial w(L_h\xi)}{\partial \xi} g(t_0\tau) \right)\Bigg|_{\xi=-0} = \upsilon(\tau, +0) \quad (34)$$

The dimensionless constants η, a, l_c and q are given as

$$\eta = \sqrt{\frac{\rho_c}{\rho_h}}, \quad a = \frac{L_h}{t_0 V_A \sin|\alpha|}, \quad l_c = \frac{L_c}{L_h}, \quad q = 1 + \frac{t_0 (ca\eta)^2}{4\pi\sigma_c L_h^2} \quad (35)$$

For the typical physical parameters mentioned in chapter 4 with $L_h = 1$ m, $\rho_c = 12 m_p n_{ci}$ and $\rho_h = 2 m_p n_h$, and using the pressure balance equation given there the constants K, s, μ, η, A and q are obtained as

$$K = 1.2, \ s = 1.4, \ \mu = 1.1\cdot 10^{-2}, \ \eta = 14, \ a = 1/140, \ q = 1 + 2.5\cdot 10^{-5} \quad (36)$$

In these estimations the conductivity is expressed as $\sigma_c = e^2 n_{ce} \tau_{ce}/m_e \approx 3\cdot 10^{14}$ s^{-1}. The electron-ion collision time in the cold plasma is given as $\tau_{ce} = 3.5\cdot 10^4 (T_c)^{3/2}/(Z n_{ce}) \approx 2\cdot 10^{-10}$ s with T_c in electronvolts. The stopping length is given as $\lambda_e = \upsilon_{The} \tau_s \approx 6$ m with $\upsilon_{The} \approx 3\cdot 10^9$ cm/s and $\tau_s = \tau_{ce}(T_h/T_c)^{3/2} \approx 2\cdot 10^{-7}$ s.

5.1 Solution of the equations

For the function w given by Eq. (25), the system of Eqs. (31), (32), (33) and (34) is solved by separation of variables. The function g is given as $g = g_p \exp(p\tau)$ with the coefficient g_p depending on the separation parameter p. The variables υ and b are

represented similarly as $\upsilon = \upsilon_p \exp(p\tau)$ and $b = b_p \exp(p\tau)$ with υ_p and b_p functions on p and ξ. Substituting these expressions into the equations and then omitting the factor $\exp(p\tau)$ it is obtained

$$p\eta^2 a \upsilon_p = s_\alpha b_p' \quad (\xi < 0), \qquad pa\upsilon_p = s_\alpha b_p' \quad (\xi > 0) \tag{37}$$

$$b_p - \frac{b_p''}{k_c^2} = -\frac{w'' s_\alpha g_p}{ps^2} \quad (\xi < 0), \qquad b_p - \frac{b_p''}{p^2 a^2} = 0 \quad (\xi > 0) \tag{38}$$

$$b_p'\big|_{\xi=-l_c} = 0, \quad b_p\big|_{\xi=1} = 0, \quad b_p\big|_{\xi=-0} = b_p\big|_{\xi=+0} \equiv b_p(0) \tag{39}$$

$$\frac{b_p'(-0)}{k_c^2} - \frac{w'(0) s_\alpha g_p}{ps^2} = \frac{b_p'\big|_{\xi=+0}}{p^2 a^2} \tag{40}$$

with the coefficient $k_c = pa\eta/[1+p(q-1)]^{1/2}$ and the derivative $b_p'(-0) = b_p'|_{\xi=-0}$ (the stroke designates $d/d\xi$). The function w of Eq. (25) is used. The function υ_p is excluded from Eqs. (38), (39) and (40).

Assuming $|p|(q-1) << 1$ and considering Eq. (38) with zero right hand side (rhs) and $p = -\mathrm{i}\omega$ with a real ω, at $\xi < 0$ the solutions with $b(\tau,\xi) \propto \exp(\pm \mathrm{i} a\eta\omega\xi - \mathrm{i}\omega\tau)$ and at $\xi > 0$ with $b(\tau,\xi) \propto \exp(\pm \mathrm{i} a\omega\xi - \mathrm{i}\omega\tau)$ are obtained. These solutions describe the sinusoidal Alfven modes of the plasmas. In the physical units the phase velocity of the modes is obtained as $\upsilon_c = B_0/(4\pi\rho_c)^{1/2}\sin|\alpha|$ at $x < 0$ and $\upsilon_h = V_A \sin|\alpha|$ at $x > 0$. Thus the modes propagate in the plasmas with the Alfven velocity along the magnetic field lines.

At $\xi > 0$ the problem is solved as $b_p = b_p(0)\mathrm{sh}[pa(1-\xi)]/\mathrm{sh}(pa)$. Thus the rhs of Eq. (40) is equal to $-b_p(0)/A$ with $A = pa\,\mathrm{th}(pa)$.

If the boundary condition $V_y|_{x=Lh} = 0$ would be used then the condition $(db_p/d\xi)|_{x=Lh} = 0$ is valid. For such case it is obtained $b_p = b_p(0)\mathrm{ch}[pa(1-\xi)]/\mathrm{ch}(pa)$ thus the rhs of Eq. (40) is equal to $-b_p(0)/A_1$ with $A_1 = pa\,\mathrm{cth}(pa)$.

At $\xi < 0$ general solution of Eq. (38) is given as

$$b_p = b_p(0)\mathrm{ch}(k_c\xi) + b_p'(-0)\frac{\mathrm{sh}(k_c\xi)}{k_c} + \frac{s_\alpha g_p k_c}{ps^2}\int_0^\xi w''(\xi_1)\mathrm{sh}(k_c(\xi-\xi_1))d\xi_1 \tag{41}$$

Substituting b_p of Eq. (41) into the boundary conditions Eqs. (39) and (40), linear equations for $b_p(0)$ and $b_p'(-0)$ are obtained. Solving these equations results in the final expression for b_p as $b_p = s_\alpha g_p G_p$ with the Green function $G_p(\xi)$ being the solution for $g_p \equiv 1$ and given as

$$G_p(\xi)=\frac{k_c}{ps^2}\left(\begin{array}{l}\dfrac{A\mathrm{ch}(k_c\xi)-k_c\mathrm{sh}(k_c\xi)}{A\mathrm{sh}(k_cl_c)+k_c\mathrm{ch}(k_cl_c)}\displaystyle\int_0^{-l_c}w''(\xi_1)\mathrm{ch}(k_c(\xi_1+l_c))d\xi_1\\ +\dfrac{Aw'(0)\mathrm{ch}(k_c(\xi+l_c))}{A\mathrm{sh}(k_cl_c)+k_c\mathrm{ch}(k_cl_c)}+\displaystyle\int_0^{\xi}w''(\xi_1)\mathrm{sh}(k_c(\xi-\xi_1))d\xi_1\end{array}\right) \quad (42)$$

Hence at $\xi > 0$ the solution is given as $b_p(\xi) = s_\alpha g_p G_p(0)\mathrm{sh}[pa(1-\xi)]/\mathrm{sh}(pa)$. According to Eq. (37) the function υ_p at $\xi < 0$ is obtained as $\upsilon_p = g_p G_p'/(p\eta^2 a)$ and at $\xi > 0$ as $\upsilon_p = -g_p G_p(0)\mathrm{ch}[pa(1-\xi)]/\mathrm{sh}(pa)$. In case of the boundary condition $V_y|_{x=Lh} = 0$ in Eq. (42) the parameter A should be replaced by the parameter A_1.

5.2 Sudden start of the plasma interaction

In case of $g(t) = \theta(t)$ the function g is represented by the Laplace integral as

$$g=\frac{1}{2\pi\mathrm{i}}\int_{-\mathrm{i}\infty}^{+\mathrm{i}\infty}\frac{\exp(p\tau)}{p}dp \quad (43)$$

thus $g_p = 1/p$. As a result the solutions for b and υ are given as

$$b(\tau,\xi)=\frac{s_\alpha}{2\pi\mathrm{i}}\int_{-\mathrm{i}\infty}^{+\mathrm{i}\infty}\left[\begin{array}{ll}G_p(\xi), & \xi<0\\ G_p(0)\dfrac{\mathrm{sh}(pa(1-\xi))}{\mathrm{sh}(pa)}, & \xi>0\end{array}\right]\frac{\exp(p\tau)}{p}dp \quad (44)$$

$$\upsilon(\tau,\xi)=\frac{1}{2\pi\mathrm{i}}\int_{-\mathrm{i}\infty}^{+\mathrm{i}\infty}\left[\begin{array}{ll}G_p'(\xi)/(p\eta^2a), & \xi<0\\ -G_p(0)\dfrac{\mathrm{ch}(pa(1-\xi))}{\mathrm{sh}(pa)}, & \xi>0\end{array}\right]\frac{\exp(p\tau)}{p}dp \quad (45)$$

As was mentioned in chapter 4, t is assumed to be small enough for neglecting of the influence of the boundaries at $\xi = -l_c$ and $\xi = 1$. Thus it is assumed that the solutions are analyzed at $|\xi| << \min(l_c,1)$. This case is met at $|p|a >> 1$ and $k_c l_c >> 1$, which is assumed below. In the time scale the inequality $|p|a >> 1$ corresponds to $\tau << a$ thus $t << at_0 \approx 0.7$ μs. Due to the small value of the parameter $q - 1$ (see Eq. (36)) below for the sake of simplicity it is assumed that additional restriction $q - 1 << 1/|p|$ is valid, which allows to neglect the term $|p|(q - 1)$. Thus the switching on process occurs during a negligibly short time Δt for which it is valid $\Delta t >> (q - 1)t_0 \approx 2$ ns. The neglecting of the term $|p|(q - 1)$ means neglecting of diffusion of the cold plasma across the magnetic field lines compared to its lateral motion. The expression for k_c is simplified as $k_c = pa\eta$ thus l_c is large as $l_c >> 1/(pa\eta)$.

At $a|p| >> 1$ and $k_c l_c >> 1$ it is valid $A \approx ap$ and $\mathrm{sh}(k_c l_c) \approx \mathrm{ch}(k_c l_c) \approx \exp(k_c l_c)/2$. At the additional condition $|\xi| << l_c$ Eq. (42) is simplified as

$$G_p(\xi)=\frac{k_c}{ps^2}\left(-k_c\frac{\mathrm{ch}(k_c\xi)-\eta\,\mathrm{sh}(k_c\xi)}{1+\eta}\int_0^{-\infty}w'(\xi_1)e^{k_c\xi}d\xi_1+k_c\int_0^{\xi}w'(\xi_1)\mathrm{ch}(k_c(\xi-\xi_1))d\xi_1\right)$$

Because $s \sim 1$, it is valid $s|\xi| << 1$. In this region the function w' is approximated as $w' \approx w'(0)$. Final simplified expression for $G_p(\xi)$ with the available condition $\eta >> 1$ is obtained as $G_p(\xi) \approx a(K/s)\exp(a\eta\xi p)$. Using this expression in Eq. (44), which is additionally simplified at $\xi > 0$ as $\mathrm{sh}(pa(1-\xi))/\mathrm{sh}(pa) \approx \exp(-a\xi p)$, and making the inverse Laplace transformation the magnetic field is obtained as

$$b(\tau,\xi)\approx\frac{s_\alpha aK}{s}\theta(\tau+a\eta\xi)\theta(\tau-a\xi) \tag{46}$$

Such solution represents the dynamics of the perturbation of the magnetic field as caused by the sudden switching on of the current generation. The perturbation propagates away from the boundary as the pulse function. Replacing the dimensionless variables τ and ξ by t and x according to Eq. (30) it is obtained that the perturbation front propagates in the hot plasma with the velocity $V_A\sin\alpha$ thus with the Alfven velocity along the lines of the magnetic field $\mathbf{B}_0$. In the cold plasma the perturbation front propagates along $\mathbf{B}_0$ with their Alfven velocity as well.

Similar behavior gets the lateral velocity. From Eq. (45) υ is obtained as

$$\upsilon(\tau,\xi)=\frac{aK}{s}\begin{bmatrix}\eta^{-1}\theta(\tau+a\eta\xi), & \xi<0\\ -\theta(\tau+a\eta\xi), & \xi>0\end{bmatrix} \tag{47}$$

Thus the lateral deflection has opposite direction for the hot and the cold plasmas. The magnitude of the lateral velocity of the hot plasma is much larger (by the parameter $\eta >> 1$) than that of the cold plasma.

Hence after the sudden start the induced self-consistent electromagnetic field propagates as the pulse having the sharp front with the Alfven velocity along the magnetic field lines into the hot plasma. A similar wave propagates in the cold plasma backward of the x-axis. In reality the wave front achieves the hot plasma edge in a time $L_h/(V_A\sin|\alpha|)$ much smaller than t_0. Due to reflection from the edge plasma modes of rather high frequencies and amplitudes would occur. The excitation of these modes results from the initial conditions at $t = 0$ only. For the above mentioned typical parameters the Alfven velocity is obtained as $V_A \approx 10^9$ cm/s. Using the value $L_h = 1$ m the relation of t_0 to the time of the mode propagation through the plasmas is estimated as $a^{-1} \sim 10^2$. Thus the mode frequencies are of the order of $1/(t_0a)$, which doesn't relate with the characteristic time t_0 of the problem under consideration. Similar remarks concern the cold plasma.

Therefore more reasonable is a model with the adiabatic increase of the interaction intensity in which the characteristic time of the switching on of the plasmas interaction is of the order of t_0. In this case the amplitudes of the high frequency parasitic modes become negligibly small if t_0 is much larger than their oscillation period. In this

case the deflection velocity at each moment depends only on the intensity of the current generator. An adiabatic solution slowly changing in space and time is obtained in the next chapter thus demonstrating the way of avoiding of the non-physical solutions.

5.3 Adiabatic increase of the interaction intensity

The case of $g(t) = \exp(\tau)$ directly corresponds to the obtained in chapter 5.1 solution with $p = 1$ and $g_p = 1$. In accordance with Eq. (36), because $q \approx 1$, it is valid $k_c = a\eta << 1$ thus at $\xi > 0$ in the stopping region of the hot electrons ($s|\xi| \sim 1$) it is valid $k_c|\xi| << 1$. At $\xi > 0$ it is valid $a\xi << 1$. The parameter A is equal to a^2. It is assumed that it is valid $k_c l_c << 1$ because at larger thickness of the cold plasma the Alfven waves generated at the separation boundary don't reach the wall in time t of the order of t_0. Due to this limitation the simplifications $\mathrm{sh}x \approx x$ and $\mathrm{ch}x \approx 1+x^2/2$ are used. Initially Eq. (42) is conveniently transformed without using the mentioned simplifications and resulting in

$$b(\tau,\xi) = \frac{a\eta\exp(\tau)}{s_\alpha s^2}\left(\begin{array}{l}\dfrac{a\mathrm{ch}(k_c\xi)-\eta\mathrm{sh}(k_c\xi)}{a\mathrm{sh}(k_c l_c)+\eta\mathrm{ch}(k_c l_c)}\left(w'(-l_c)+k_c^2\displaystyle\int_0^{-l_c} w(\xi_1)\mathrm{ch}(k_c(\xi_1+l_c))d\xi_1\right)\\ +k_c w(\xi)+k_c^2\displaystyle\int_0^{\xi} w(\xi_1)\mathrm{sh}(k_c(\xi-\xi_1))d\xi_1\end{array}\right) \quad (48)$$

Then the integral terms are neglected because of the small factor $(k_c)^2$. After using the simplifications it is obtained

$$b(\tau,\xi) \approx s_\alpha \frac{a^2}{s^2}\exp(\tau)\left(\frac{1-\eta^2\xi+\frac{1}{2}a^2\eta^2\xi^2}{1+a^2 l_c}w'(-l_c)+\eta^2 w(\xi)\right) \quad (\xi < 0) \quad (49)$$

The function b of Eq. (49) meets the boundary condition $b'(-l_c) = 0$ exactly. Thus it represents adequately the adiabatic solution at $\xi < 0$.

According to Eq. (49) the magnitude of the magnetic field at the separation boundary is given as $b(\tau,0) \approx (a/s)^2\exp(\tau)w'(-l_c)$. Thus its behavior at $\xi > 0$ is obtained as

$$b(\tau,\xi) \approx s_\alpha \frac{a^2}{s^2}\exp(\tau)w'(-l_c)(1-\xi) \quad (\xi > 0) \quad (50)$$

According to Eq. (37) the lateral velocity is given as

$$\upsilon(\tau,\xi) = \frac{a}{s^2}\exp(\tau)\left[\begin{array}{ll} w'(\xi)-\dfrac{1-a^2\xi}{1+a^2 l_c}w'(-l_c), & \xi < 0\\ -w'(-l_c), & \xi > 0\end{array}\right] \quad (51)$$

Comparing Eqs. (46) and (49) it is concluded that the magnitude of the magnetic field in the adiabatic case at the final moment $t = 0$ is much less (by the parameter $a << 1$) compared to the case with the sudden start. Comparing Eqs. (47) and (51) it is concluded that the lateral velocity of the hot plasma in both situations is of the same magnitude at $sl_c << 1$ and is smaller in the adiabatic case by the factor $w'(-l_c) << 1$ at $sl_c > 1$.

In physical units and with w given by Eq. (25) the lateral velocity is given as

$$V_y \approx \frac{V_A \mu a K e^{t/t_0 - sl_c}}{s\left(1+K\left(1-e^{-sl_c}\right)\right)}\left(\frac{1+K\left(1-e^{-sl_c}\right)}{1+K\left(1-e^{s\xi}\right)}e^{s(\xi+l_c)}\theta(-x)-1\right) \tag{52}$$

In accordance with Eq. (9) the lateral deflection is given as $\Delta_y = t_0 V_y$. At the final time moment $t = 0$ the deflection magnitude of the plasmas at $x = \pm 0$ is different and given as

$$\Delta_y\Big|_{\substack{t=0\\ x\to\pm 0}} \approx \frac{t_0 V_A \mu a K}{s}\left(\theta(-x)-\frac{e^{-sl_c}}{1+K\left(1-e^{-sl_c}\right)}\right) \tag{53}$$

A typical behavior of the induced magnetic field and of the deflection velocity is demonstrated in Fig. 4 and Fig. 5. The dependence of the deflection on the thickness of the cold plasma is shown in Fig. 6.

From Eq. (53) follows that at $sl_c >> 1$ the deflection of the hot plasma being determined by the factor $\exp(-sl_c)$ becomes negligibly small. In this case, which is not analyzed here, the integral terms neglected in Eq. (48) are significant for the deflection effect. Maximal magnitudes of the hot plasma deflection are produced at $sl_c <<1$. In this case the magnitude Δ_h of the hot plasma deflection is larger than the magnitude Δ_c of the cold plasma. According to Eq. (53) at $sl_c <<1$ the relation of the magnitudes is given as $\Delta_c/\Delta_h \approx (K+1)sl_c$. At $sl_c <<1$ for the mentioned above typical values of the plasma parameters and in accordance with Eqs. (36) and (53) the deflection magnitude of the hot plasma is obtained as $\Delta_h \approx 7$ cm. The behavior of Δ_h at $sl_c <<1$ as function of the plasma parameters is given as

$$\Delta_h[\mathrm{cm}] \approx \frac{0.7Z}{5\tan|\alpha|}\exp\left(1-\frac{e\phi_0}{T_h}\right)\frac{t_0}{10^2\,\mu s}\left(\frac{30\mathrm{eV}}{T_c}\right)^{\frac{3}{2}}\frac{5\mathrm{T}}{B_0}\left(\frac{T_h}{3\mathrm{keV}}\right)^{\frac{1}{2}}\frac{n_h}{3\cdot 10^{13}\,\mathrm{cm}^{-3}} \tag{54}$$

In case of the boundary condition with $\upsilon(\tau,1) = 0$ it is obtained similarly:

$$b(\tau,\xi) = \frac{\exp(\tau)}{s_\alpha s^2}\left[\begin{array}{ll} \dfrac{1+\frac{1}{2}(a\eta\xi)^2 - a^2\eta^2\xi}{1+l_c}w'(-l_c)+a^2\eta^2 w(\xi), & \xi<0 \\ \dfrac{w'(-l_c)}{1+l_c}\dfrac{\mathrm{ch}(a(1-\xi))}{\mathrm{ch}(a)}, & \xi>0 \end{array}\right] \tag{55}$$

$$\upsilon(\tau,\xi)=\frac{a}{s^2}\exp(\tau)\begin{bmatrix}\frac{\xi-1}{1+l_c}w'(-l_c)+w(\xi), & \xi<0\\ -\frac{w'(-l_c)}{1+l_c}\frac{\mathrm{sh}(a(1-\xi))}{a\mathrm{ch}(a)}, & \xi>0\end{bmatrix} \tag{56}$$

Comparing Eq. (55) with Eqs. (49) and (50) it is concluded that in case of the fixed boundary of hot plasma the magnitude of B_y in the hot plasma is by a factor $1/a^2$ larger than that one in case with the free boundary. Thus in the case of the fixed hot plasma boundary the induced magnetic field in the hot plasma remains rather small being of 0.2 T for the above mentioned values of the plasma parameters. Comparing Eq. (56) with Eq. (51) it is concluded that the lateral velocities, thus the lateral shifts of the plasmas, don't differ significantly for the both cases.

6. DISCUSSION

In chapter 5 the assumption that B_y is small is used in order to provide the linear character of the analyzed problem. Estimating B_y in case of the adiabatic increase of the interaction intensity according to Eq. (50), it is obtained that at the final moment $t = 0$ and at the small thickness of the cold plasma ($L_c << \lambda_e \sin\alpha$) it is valid $B_y = B_0\mu b(0) \sim B_0\mu a^2K/s \approx 0.02$ G for $B_0 = 5$ T and the values of the dimensionless parameters mentioned in Eq. (36). But as it is shown, despite such small values of the induced magnetic field, the lateral deflection of the hot plasma, which occurs only due to non-zero B_y, is of the order of the experimentally measured values.

The last term in the exponent of Eq. (24) can be neglected if it is much less than one. Using Eq. (50) this vortex field term conveniently estimated as $(q-1)sK\cos^2\alpha$ is approximately equal to 10^{-4}. Thus the solution $w(x)$ given by Eq. (20) is justified. The small contribution of the vortex electric field to φ makes the effective potential equal to the usual electric potential with a good accuracy. Hence the electric stopping of the hot electrons in the inclined magnetic field is practically the same as that of the perpendicular impact.

The contribution of the **E**×**B** drift term in $\mathbf{J}_{he}$, which is expressed by the function ΔE_z of Eq. (22), in comparison with the lateral velocity is defined as $|c\Delta E_z/(B_xV_y)|$. For estimation of the contribution the value $|b| \approx a^2K/s$ given by Eqs. (50) at $l_c << 1$, $\tau = 0$ and $\xi = 0$ is used. From Eq. (37) at $p = 1$ it is obtained $|(\partial b/\partial\xi)/\upsilon| = \eta^2 a$. According to Eq. (5) at $x = 0$ it is valid $n_{he} = n_h/2$. The dimensionless parameters are conveniently used. As a result it is obtained

$$\left|\frac{\Delta E_z}{B_xV_y/c}\right| \sim \frac{T_c}{4T_h}\left(1+\frac{1}{Z}\right)\left(1+\frac{\mu\cot|\alpha|a^2K}{\tau_{ce}\omega_e s}+2(q-1)\sin^2\alpha\right)$$

with $\omega_e = eB_0/m_e c$ the electron gyro-frequency and τ_{ce} the electron-ion collision time, which is calculated in chapter 5 as $\tau_{ce} \approx 2\cdot 10^{-10}$ s. At $B_0 = 5$ T it is valid $\omega_e \approx 10^{12}$ s^{-1}. Thus the neglect of the drift term is correct because it is valid $|c\Delta E_z/(B_x V_y)| << 1$.

The parameter K is reversely proportional to the conductivity σ_c of the cold plasma. Thus according to Eq. (53) if the cold plasma would be a perfect conductor, the deflection would not occur because $\Delta_y \to 0$ at $\sigma_c \to \infty$. This confirms the discussion of chapter 4.1 on the physical nature of the lateral effect.

Below the first four of the experimental facts mentioned in chapter 3 are discussed in their relation to the considered model.

The observation that the deflection occurs only due to the inclination of the magnetic field is met in the presented model. According to Eq. (54) the magnitude of the deflection contains the inclination angle α in the factor $1/\tan|\alpha|$. Thus the larger the inclination (the smaller α) the larger the deflection. Without inclination (at perpendicular impact with $\alpha = 90^{\circ}$) the factor $1/\tan|\alpha|$ gets equal to zero, which results in vanishing of the lateral deflection.

The observation that the strike points move mainly before the power flux pulse arrives correlates well with the model because it is obtained that the deflection of the hot plasma develops most effectively at thin vapor shield and at small temperature T_c of the cold plasma. According to Eq. (51) the lateral velocity of the hot plasma is proportional to the factor $w'(-l_c) \sim \exp[-L_c/(\lambda_e \sin|\alpha|)]$. Thus when increasing the thickness L_c of the vapor shield the lateral velocity decreases. According to Eq. (54) the deflection is proportional to $(T_c)^{-3/2}$. In the adiabatic switching on regime the same is valid for the lateral velocity. In the vapor shield simulations T_c is smaller in the initial phase of the plasma-target interaction than at the main phase. Thus the model reasonably describes the faster deflection at the initial stage because of the lower vapor shield temperature. Eq. (54) describes also the dependence of the deflection on the temperature T_h and the density n_h of the hot plasma. The value of T_h due to cooling of the cold plasma may get to decrease in time. Such possible dynamics of T_h doesn't collide with the result of Eq. (54) that the smaller T_h the smaller the lateral velocity.

The observation that the higher the power density the larger the deflection is also in agreement with the model. According to Eq. (54) the deflection is proportional to n_h, which stagnates rather soon after hot ions arrive to the wall.

The magnitude of deflection obtained in the model is in reasonable agreement with the experimental results.

In the frame of the considered model it is impossible to explain the observation that the strike points move in the opposite directions. Formally the situation near the inner and the outer strike points differs by the sign of α. But according to Eq. (54) the deflection is expressed by the even function of α. Therefore the change of the sign is not followed by the change of the direction of the deflection, which doesn't agree with the experiment.

The choice of the boundary condition at the hot plasma edge in the considered problem seems reasonable, which follows from experiments. If would favor the opposite direction of the shifts of the strike points, the symmetrical boundary condition with $(\partial V_y/\partial x)|_{x=Lh} = 0$ seems in advance more reasonable. However such a choice contradicts the obtained asymmetry of the solutions as function of the direction of the poloidal

magnetic field, which is expressed by the even dependence on the angle α in Eq. (54). If believing for the asymmetry, the condition $V_y|_{x=Lh} = 0$ seems more preferable. But definitely this question is not answered by the carried out one-dimensional analysis.

7. CONCLUSION

SOL plasma deflection may play a significant role in the problem of hot plasma-solid wall interaction because the exposition area of the hot plasma is increased and because an additional mechanism of the cold plasma removal from the exposed area is developed. Due to the removal of the cold plasma the effectiveness of the vapor shield may get less effective, which can cause enhanced wall erosion despite the decrease of the average power density of the hot plasma target irradiation.

Despite rather significant mathematical simplifications of the considered process of the plasma-target interaction, which was necessary for the development of the analytical model for the deflection effect, the approach seems fruitful. The quantitative agreement and the qualitative similarity of the theoretical and the experimental results bring the hope that the suggested physical picture is relevant to the real deflection phenomenon. Nevertheless additional theoretical ideas are necessary for explanation of the directions of the deflection. The still rather artificial one-dimensional model considered in this work may be useful for the development of a more adequate one- and two-dimensional numerical simulation of the target-plasma interaction with accounting for the lateral deflection of both the hot SOL plasma and the vapor shield layer.

8. REFERENCES

1. M. Keilhacker, M.L. Watkins, JET Team, 'D-T experiments in the JET tokamak', J. Nucl. Mater., 266-269, 1, (1999)
2. H. Wuerz, B. Bazylev, I. Landman, S. Peschanyi, 'Vapor shielding and erosion of walls during tokamak disruptions', Nucl. Instr. & Metods in Phys. Research, A 415, 543 (1998)
3. J. Lingertat, A. Tabasso, S. Ali-Arshad, B. Alper, P. Van Belle, K. Borrass, S. Clement, J.P. Coad and R. Monk, 'Stadies of giant ELM interaction with the divertor target in JET', J. Nucl. Mater., 241-243, 402, (1997)
4. L.L. Lengyel, V.A. Rozhanskij, I.Yu. Veselova, P.J. Lalousis, 'Drift motions in the scrape-off layer during hard disruptions', Nucl. Fus., 37, 1245 (1997)
5. I. Landman, H. Würz, In 24th Conference on Controlled Fusion and Plasma Physics (European Physical Society, Berchtesgaden, 1997), Vol. 21A, Part IV, p. 1821.
6. I.S. Landman, H.Würz, 'Electric fields and ExB drifts in hot plasma cold plasma interaction', FZKA 6192, Forschungszentrum Karlsruhe, 1998
7. J. Lingertat, private communication, 1999
8. H. Wuerz et al., 'Hot plasma target interaction and quantification of erosion of the ITER slot divertor during disruptions and ELMs', FZKA 6198, Forschungszentrum Karlsruhe, 1999
9. V. Safronov et al., 'First investigation on formation and existence of electric fields in hot plasma cold target plasma interaction', Disruption meeting in St-Petersburg, NIIEFA, November 24-26, 1997
10. V.A. Rozhanskij and L.L Lengyel, 'Calculation of electrostatic fields in vapor shields evolving at ablating surfaces', IPP 5/33, Max-Planck-Institut für Plasmaphysik, Garching, 1993

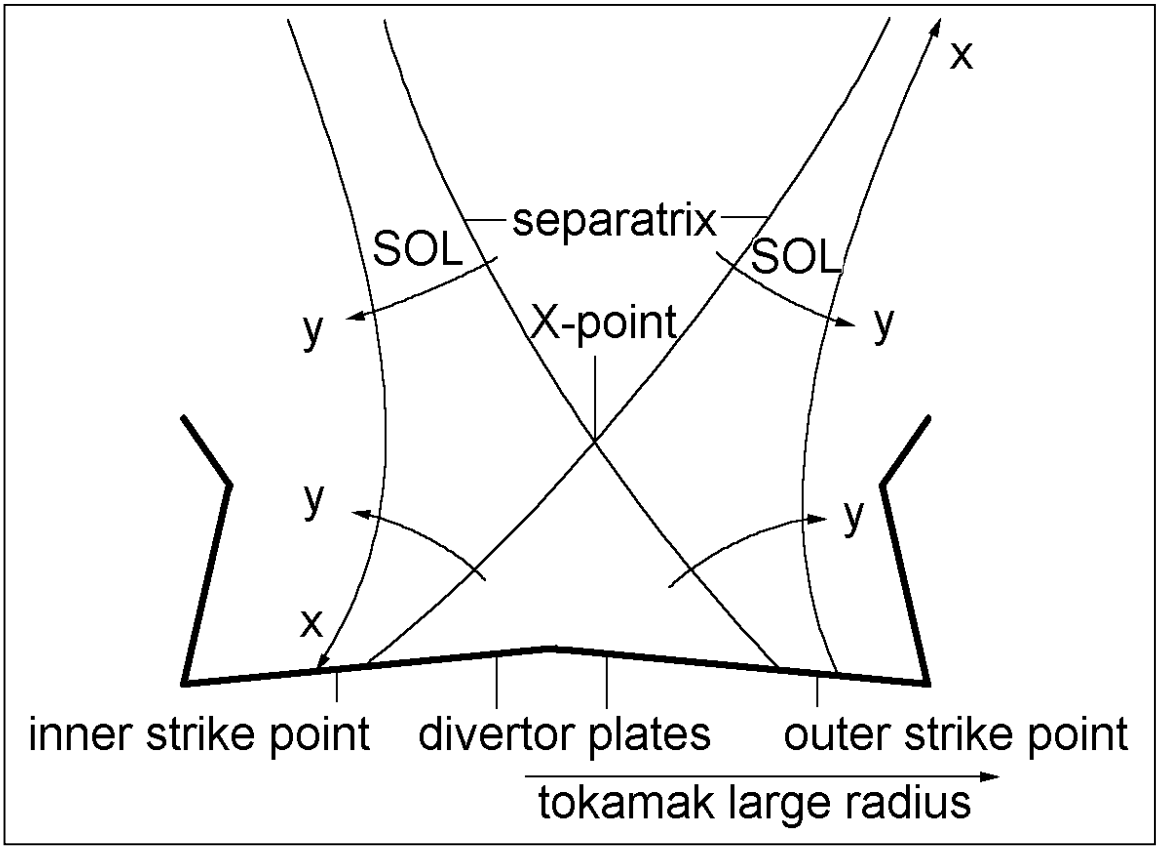

Fig. 1. The divertor and the geometry of the SOL schematically. The strike points of the SOL plasma are located at the divertor plates. The curvilinear magnetic flux coordinates *x* and *y* are assumed to be orthogonal. The toroidal coordinate *z* (not shown) is orthogonal to *x* and *y*. The separatrix separates the confined plasma from the SOL region. In the X-point the magnetic field has only a toroidal component but no poloidal one. The poloidal magnetic field lines indicate the separatrix and the *x*-axis.

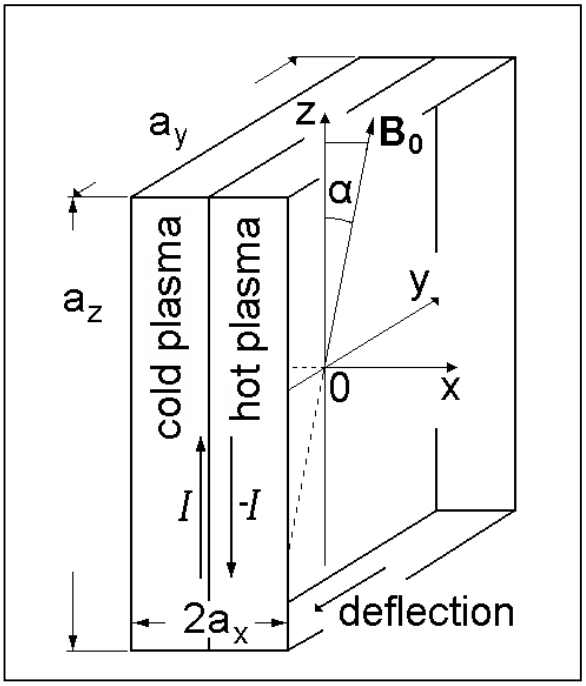

Fig. 2. Positions of the plasmas schematically. a_x, a_y and a_z are the plasma sizes with a_x shown in the figure to be equal for both plasmas. Compensating toroidal currents I and $-I$ are developing in the hot cold plasma interface. The lateral deflection develops in y-direction.

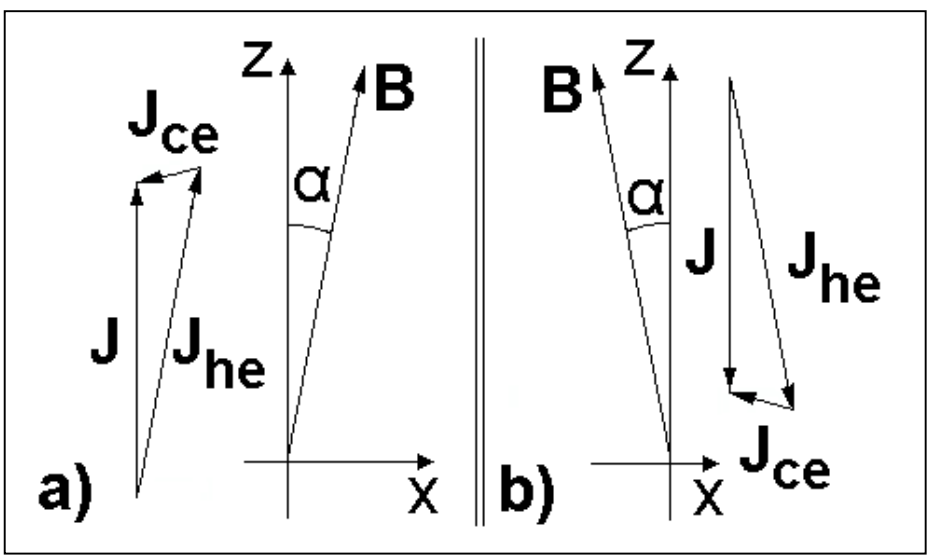

Fig. 3 The non-compensated hot and cold electron current density $\mathbf{J}_{he}$ and $\mathbf{J}_{ce}$ in the cold plasma schematically. $\mathbf{J}$ is the resulting toroidal current density. a) $B_x > 0$, b) $B_x < 0$. Note that the electron current density vector is opposite to the vector of electron number flux.

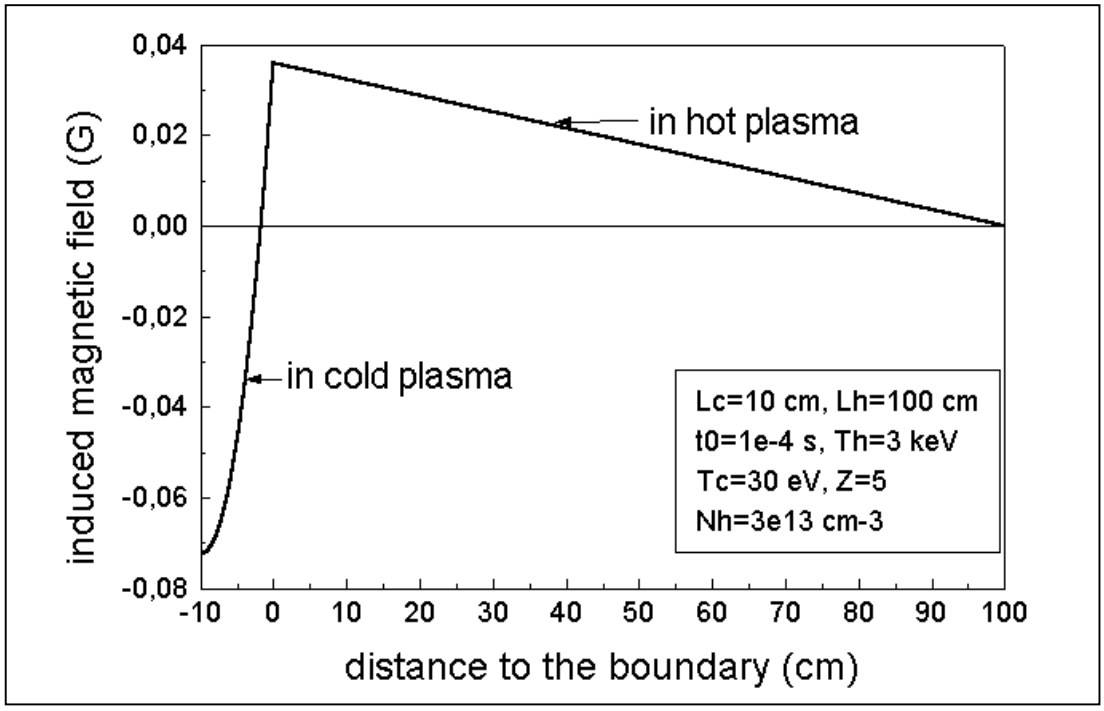

Fig. 4 Distribution of the induced magnetic field after 100 μs.

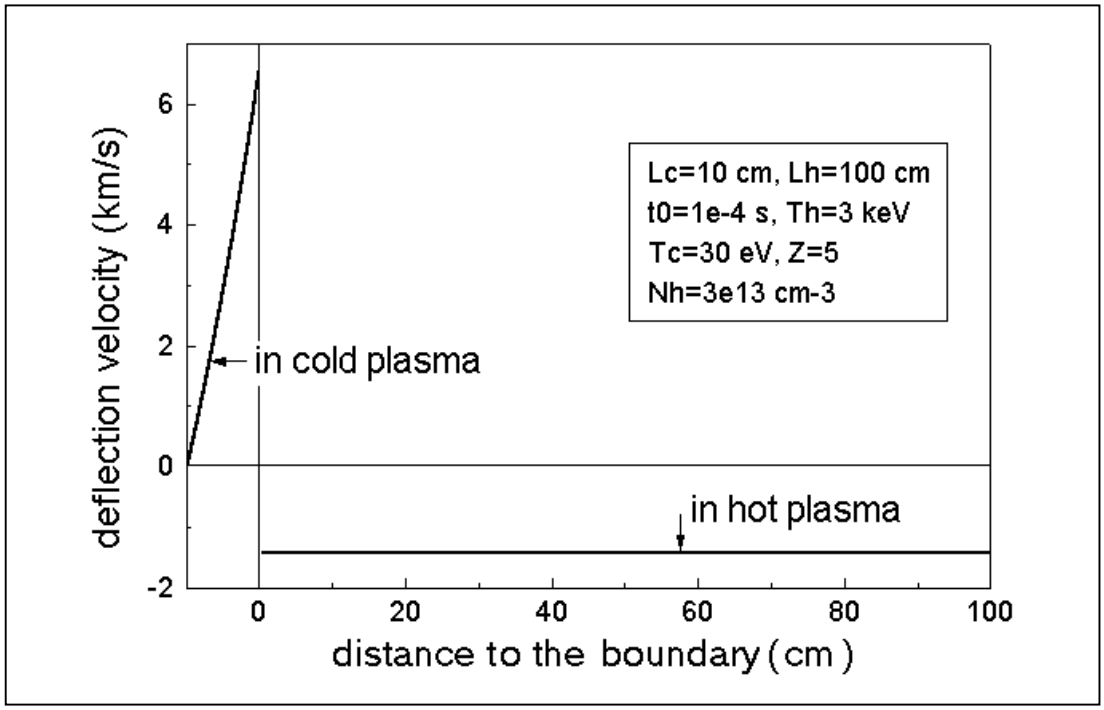

Fig. 5 Deflection velocity after 100 μs.

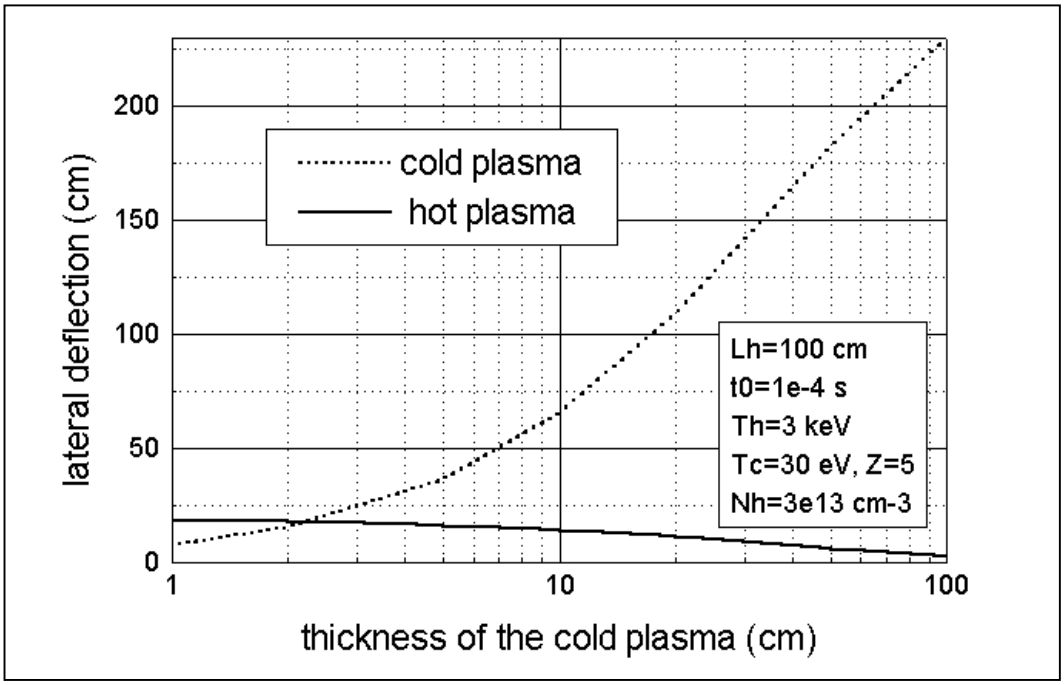

Fig. 6 Deflection of the plasmas after 100 μs as function of the cold plasma thickness.